Kinetics of electron attachment to OH and HNO_3 and mutual neutralization of Ar^+ with NO_2^- and NO_3^- at 300 and 500 K

Nicholas S. Shuman, Thomas M. Miller, and A. A. Viggiano

Citation: The Journal of Chemical Physics **136**, 124307 (2012); doi: 10.1063/1.3694876
View online: https://doi.org/10.1063/1.3694876
View Table of Contents: http://aip.scitation.org/toc/jcp/136/12
Published by the American Institute of Physics

Kinetics of electron attachment to OH and HNO_3 and mutual neutralization of Ar^+ with NO_2^- and NO_3^- at 300 and 500 K

Nicholas S. Shuman, Thomas M. Miller, and A. A. Viggiano
Air Force Research Laboratory, Space Vehicles Directorate, Kirtland Air Force Base, Albuquerque, New Mexico 87117-5776, USA

(Received 7 February 2012; accepted 29 February 2012; published online 26 March 2012)

The electron attachment rate constant to nitric acid (HNO_3) has been measured in a flowing afterglow-Langmuir probe (FALP) apparatus at 300 and 500 K using three independent methods: the traditional FALP technique of monitoring electron depletion, "one-gas" VENDAMS (variable electron and neutral density attachment mass spectrometry), and "two-gas" VENDAMS. The three measurements are in agreement with a 300 K weighted average of $1.4 \pm 0.3 \times 10^{-7}$ cm^3 s^{-1}, 2 to 10 times higher than previously reported values. Attachment is primarily dissociative yielding NO_2^- as previously reported, but for the first time a small endothermic channel to produce OH^- was also observed at 500 K. From the one-gas VENDAMS data, associative attachment to the OH produced in the primary attachment was found to occur with an effective two body rate constant of $1.2 \pm^{3}_{0.7} \times 10^{-11}$ cm^3 s^{-1} at 300 K, the first reported rate constant for this radical species. Finally, ion-ion neutralization rate constants of NO_2^- and NO_3^- with Ar^+ were determined to be $5.2 \pm^{1.5}_{2.5} \times 10^{-8}$ and $4.5 \pm 2.5 \times 10^{-8}$ cm^3 s^{-1} at 300 K, respectively. © *2012 American Institute of Physics*. [http://dx.doi.org/10.1063/1.3694876]

INTRODUCTION

The flowing afterglow Langmuir probe (FALP) with mass spectrometric detection has a long history as a valued apparatus for understanding a variety of plasma chemistry.[1–3] FALP experiments have produced accurate kinetics for ion-molecule reactions,[1,3] electron attachment to stable molecules,[4,5] and electron-ion recombination.[6] These measurements all involved monitoring the concentration of either electrons (using the Langmuir probe) or ions (using the downstream mass spectrometer) with only one unknown reaction occurring. Rate constants for ion-ion mutual neutralization (MN) of positive and negative ions have also been measured,[7] but with the complication of relying on measurements of ion concentrations using the Langmuir probe at relatively high pressure.[8]

New areas of study have recently become accessible by using an unmodified FALP apparatus in a different manner. In this new method, dubbed variable electron and neutral density attachment mass spectrometry (VENDAMS), relative anion abundances are monitored after a fixed reaction time, while varying the initial plasma density at the reactant gas inlet.[9,10] The former is measured using the mass spectrometer and the latter using the Langmuir probe. Several processes for which little or no data were previously available have been studied with this technique, including: rate constants of electron attachment to transient species, such as radicals,[10,11] accurate mutual neutralization rate constants that do not rely on absolute ion concentration measurements,[10,12] products of mutual neutralization,[11] and evidence of a new mechanism for mutual neutralization we have termed electron catalyzed mutual neutralization (ECMN).[12]

Here we report kinetics data involving electron attachment to nitric acid, HNO_3, using three experimental methods: (a) the traditional FALP technique of measuring electron depletion as a function of reaction time, (b) "one-gas" VENDAMS with only HNO_3 added to the afterglow, and (c) "two-gas" VENDAMS with both HNO_3 and CCl_4 added.

Dissociative electron attachment to HNO_3 has previously been shown to occur by[13–16]

$$e^- + HNO_3 \rightarrow NO_2^- + OH, \quad \Delta H_{298} = -0.13 \text{ eV}. \tag{1}$$

We report here for the first time a second channel that produces OH^- in an endothermic reaction[15,17]

$$e^- + HNO_3 \rightarrow OH^- + NO_2, \quad \Delta H_{298} = 0.31 \text{ eV}. \tag{2}$$

An additional channel to form NO_3^- ($\Delta H_{298} = 0.45$ eV) is sufficiently endothermic that it is not observable under our experimental conditions. The OH formed in reaction (1) can also undergo associative attachment through stabilization by collision with a buffer gas

$$e^- + OH + He \rightarrow OH^- + He, \quad \Delta H_{298} = -1.82 \text{ eV (Ref. 17)}. \tag{3}$$

In the Ar^+/e plasma employed in these experiments, all of the anions can undergo MN with Ar^+ by either a conventional mechanism or by ECMN; exemplified for NO_2^- as

$$Ar^+ + NO_2^- \rightarrow \text{neutrals}, \tag{4}$$

$$Ar^+ + NO_2^- + e^- \rightarrow \text{neutrals} + e^-. \tag{5}$$

None of the products of mutual neutralization of NO_2^- by Ar^+ attach electrons rapidly enough to detect, precluding determination of product distributions. In this paper we report rate constants for reactions (1-5) at 300 K and 500 K as well as for both forms of mutual neutralization for Ar^+ with NO_3^- and OH^-.

INSTRUMENTAL

The measurements were made using the Air Force Research Laboratory's FALP apparatus.[18] Data were obtained by both the traditional electron depletion method[5,19] and the new VENDAMS method.[10,20] In both methods, an $Ar^+(95\%)/e^-$ plasma is established by ionizing helium (1 Torr) using a microwave discharge and then adding Ar downstream at about 5% of the He flow to convert He metastables and He_2^+ to Ar^+. The remaining positive ions are mainly He^+ (∼5%) with <1% of ions due to impurities such as H_2O^+ and O_2^+. The density of the electrons is measured using a Langmuir probe movable across the final 60 cm of the 1 m flow tube.

HNO_3 is a difficult compound to deliver in accurate amounts and therefore our procedures for sample production and for measuring HNO_3 concentration in the flow tube are detailed here.[21,22] A 2:1 H_2SO_4:HNO_3 mixture is made in a glass bulb. The H_2SO_4 sequesters H_2O in the liquid phase, leaving only HNO_3 in the vapor. After several freeze pump thaw cycles, about 5 Torr of HNO_3 vapor is diluted to a known concentration of about 1% in He in a stainless steel sample vessel. The mixture is added to the afterglow through a 1 std. cm^3, all-metal flow controller (MKS Instruments), 20 cm of stainless steel tubing, and 45 cm of glass tubing (the glass tubing is internal to the flow tube to allow time for thermalization to the flow tube temperature). The derivations of rate constants are dependent on knowing the concentration of HNO_3 delivered. In principle, the known flow rates of HNO_3 and the buffer gases determine the concentration; however, any surface reaction in the inlet lines would decrease that amount. Fortunately, the concentration of HNO_3 may be conveniently monitored by the NO_3^-:NO_2^- ratio at low plasma density, with NO_3^- being produced at the 1%-3% level by

$$NO_2^- + HNO_3 \rightarrow NO_3^- + HNO_2. \quad (6)$$

The measured rate constant of this reaction (1.6×10^{-9} cm^3 s^{-1})[14] is about 25% below the collisional value of 2.2×10^{-9} cm^3 s^{-1}.[23] Generally, simple proton transfer reactions proceed at the collisional value,[24] and we expect that discrepancy is a good determination of the uncertainty in the rate constant of Eq. (6) and therefore in the derived HNO_3 concentration. The rate of NO_2^- production, reaction (1), is dependent on both the uncertain HNO_3 concentration and the unknown rate constant of electron attachment to HNO_3; the rate of reaction (6) is similarly dependent on the HNO_3 concentration and the rate of NO_2^- production. Monitored together, these two reactions provide sufficient constraint that both unknowns, $[HNO_3]_0$ and k_1 (where k_1 is the rate constant of reaction (1), electron attachment to HNO_3) may be determined.

The HNO_3 concentration was observed to vary with time. After opening the sample cylinder valve and flowing HNO_3 into the system, the concentration rose for a couple of minutes, presumably due to passivation, then stabilized for about 5 min, then slowly decreased. Closing the sample valve and then pumping on the inlet line and repeating led to behavior and concentrations that were the same as that obtained from the previous sample. For this reason, we often returned to the low plasma density condition and measured the sample concentration. Data were only taken in the ∼5 min window where the concentration was stable. In this window, the HNO_3 concentration was consistently within 10% of the nominal value determined by the reactant and buffer gas flow rates.

In the traditional FALP method, HNO_3 is added through a fixed ring inlet with four small, radial glass tubes for gas introduction. The electron density is measured as a function of distance both without and with attaching gas added. The former determines the diffusional losses and the latter the coupled effects of diffusional and attachment losses. Distance is equated to time by measuring the plasma velocity by time-of-flight, accomplished by pulsing the discharge and measuring the disturbance on the Langmuir probe. The traditional method uses an initial plasma density, $[e]_0$, of $\sim 10^9$ cm^{-3} at the neutral inlet. At such low densities the only process that occurs appreciably is electron attachment to HNO_3, and interpreting the decay of electron density with time only requires a decoupling of diffusion and attachment. Normally, the concentration of attaching gas is much greater than that of electrons and the decay is fit according to a standard equation for loss. In the present experiments, the initial HNO_3 concentration was around 10^{10} cm^{-3} and the kinetics were solved numerically accounting for loss of both electrons and HNO_3 in the reaction, although it was found that not accounting for loss of the neutral would cause negligibly small errors.

VENDAMS measurements start with the addition of one or two gases through the reactant gas inlet. Measurements are made by varying the plasma concentration at the inlet, $[e^-]_0$, from well below to well above the added neutral concentration while monitoring the relative concentrations of negative product ions 46 cm (about 4.6 ms reaction time) downstream. Relative ion concentrations are measured by sampling a portion of the gas through a 330 μm aperture into a quadrupole mass spectrometer coupled to an analog electron multiplier. Mass discrimination factors are quite important and are measured by procedures described in detail previously.[10] For context, the largest correction we have measured is factor of 3 against F^- compared to SF_6^-, with essentially no discrimination between polyatomic anions with mass below SF_6^-.[10] For the ions used here, a discrimination calibration curve was used rather than factors measured directly for the specific ions, with no discrimination assumed amongst the polyatomic anions and a factor of 1.1 against Cl^-; a 10% uncertainty in the discrimination factors is assumed and reflected in reported uncertainties.

The most straightforward VENDAMS experiment reported here is to add both HNO_3 and CCl_4 (a "two-gas" VENDAMS experiment). In this method, the CCl_4 concentration is kept relatively high ($\sim 2 \times 10^{10}$ cm^{-3}) such that the electron density is rapidly depleted through dissociative attachment to form Cl^-. A smaller amount of NO_2^- is formed through reaction (1) due to a lower concentration of HNO_3 and slower attachment. At low $[e^-]_0$, the ratio of product anions reflects the relative attachment rates; because the neutral concentrations are known along with the attachment rate constant to CCl_4,[25,26] the rate constant of attachment to HNO_3 may be simply derived. As $[e^-]_0$ increases, the Ar^+ concentration also increases and two-body mutual neutralization of Ar^+ with NO_2^- and NO_3^- becomes significant. Mutual

neutralization of Ar^+ with Cl^- occurs at a negligibly small rate.[27,28] The decrease in the NO_2^- and NO_3^- relative abundances towards higher $[e^-]_0$ reflects the difference between their mutual neutralization rate constants and that of Cl^-. Because the latter is effectively zero, the method yields absolute values for the two-body mutual neutralization rate constants.

With only HNO_3 added in low concentration (a "one-gas" VENDAMS experiment), several other processes can occur appreciably besides the chemistry described above. First, OH^- is produced by attachment to the OH radical formed in reaction (1). ECMN of Ar^+ with NO_2^- and NO_3^- occurs, as well as both types of mutual neutralization for OH^-. Ion-molecule reactions, excepting reaction (6), are unimportant due to the low neutral concentrations, although the modeling includes both positive and negative ion-molecule reactions.

For VENDAMS, the derivation of rate constants from the measured anion abundances has been described in detail in Ref. 12. The concentrations of species in the system throughout a fixed reaction time are characterized by the known initial conditions and by the set of possible reactions between species known (observed ions) or inferred (corresponding neutrals) to be present in the flow tube. In addition to the electron attachment and mutual neutralization reactions described above, these include charge transfer from Ar^+ to neutral species including H_2O and recombination of electrons and polyatomic cations. Although many reactions are included in the modeling, only the fastest reactions involving the most abundant species, namely, the electron attachment and mutual neutralization reactions described above, have any measurable effect on the relative anion abundances. The exception is that the HNO_3 displaces a Cl-containing species from the walls of the inlet line, resulting in a Cl^- background in the data from subsequent dissociative attachment to the contaminant. Over the course of a single experiment, the Cl^- signal was constant. Over a number of days, the Cl^- signal decreased but never went to zero. The background signal is included in the modeling by allowing dissociative attachment to an unknown species XCl and allowing both the attachment rate constant and XCl concentration to vary freely. Data taken with various amounts of the impurity yielded the same rate constants within error.

Although numerically calculating the relative anion abundances expected from a particular set of initial conditions and reaction rate constants is straightforward, the possible parameter space defined by all possible rate constants and uncertainty in the initial reactant concentrations is quite large. As described in Ref. 29 a Monte Carlo optimization procedure is used to derive both best-fit values and uncertainties for rate constants and initial conditions. The rate constants of all reactions, including those that do not significantly affect the derived values, are varied over ranges limited only by calculated collisional rate constants[26,30] or, where possible, values from the literature. For each set of possible initial conditions the final anion abundances are calculated by iteratively solving the set of coupled differential equations describing the production and destruction of each species. The calculated abundances are compared to the experimental values via a weighted least square goodness-of-fit. The best-fit value of each rate constant is determined by the minimum in a plot of the goodness-of-fit as a function of that particular rate constant. Uncertainty limits are determined by the extreme values of that rate constant yielding the worst goodness-of-fit still providing a reasonable description of the data as judged by eye.

RESULTS AND DISCUSSION

Figure 1 shows typical one-gas VENDAMS data sets at 300 and 500 K. For simplicity, the Cl^- impurity is left out of the figure but is similarly well-modeled. Typical XCl concentrations were on the order of 1% of the HNO_3 concentration with an effective attachment rate constant of $\sim 1 \times 10^{-7}$ cm^3 s^{-1}. In VENDAMS data, relative abundances of anions produced in a primary electron attachment, e.g., reactions (1) and (2), will have zero slope as a function of $[e]_0$ at lower $[e]_0$, and may show curvature at higher $[e]_0$ due to MN or other reactions. Relative abundances of anions produced

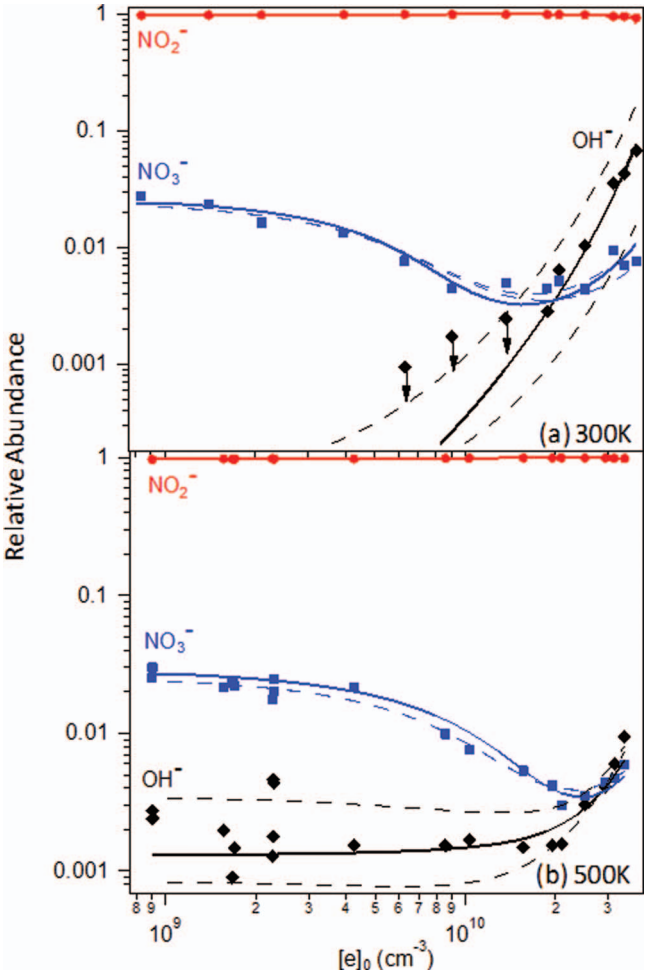

FIG. 1. "One-gas" VENDAMS data from addition of 3.8×10^9 cm^{-3} HNO_3 to the afterglow at (a) 300 K and (b) 500 K. Experimental (points: NO_2^-, red circles; NO_3^-, blue squares; OH^-, black diamonds) and calculated (best-fit, solid lines; at uncertainty limits for (a) k_3 ($OH + e \rightarrow OH^-$) and (b) k_2 ($HNO_3 + e \rightarrow NO_2 + OH^-$), dashed lines; see Table I) relative anion abundances after 4.6 ms reaction time vs. initial electron density. The Cl^- impurity is left off the graph for clarity.

in secondary attachment, e.g., reaction (3), will have positive slopes as a function $[e]_0$, rising roughly linearly with $[e]_0$.

At 300 K (Fig 1(a)), NO_2^- is the dominant anion for the complete range of $[e^-]_0$. The NO_3^- relative abundance is a few percent at low $[e^-]_0$, and decreases as $[e^-]_0$ increases above $\sim 5 \times 10^9$ cm^{-3}. Finally at high density, the NO_3^- relative abundance increases again. The initial decrease is due to the HNO_3 being depleted by electron attachment, reaction (1), and therefore slowing the NO_2^- conversion to NO_3^-, reaction (6). The increase in NO_3^- is a result of the mutual neutralization rate of NO_3^- with Ar^+ being slower than that for NO_2^-. OH^- is also observed, increasing dramatically at $[e^-]_0 > 10^{10}$ cm^{-3}. The positive slope indicates that the OH^- signal is the result of a secondary process, likely attachment to OH, reaction (3). The modeling does not reproduce the lowest concentration points. However, those OH^- mass peaks are of low intensity and we treat the abundances as upper limits. The data can be fit at these low levels somewhat better if reaction (2) is included in the modeling with a rate constant of about 1×10^{-10} cm^3 s^{-1}; however, its endothermicity indicates that the rate constant for that process cannot be greater than 5×10^{-12} cm^3 s^{-1} at 300 K. An alternative explanation for the OH^- increase involves producing NO in the neutralization of NO_2^- and then HONO formation by association of OH and NO and finally dissociative attachment to HONO; however, the known rate of reactivity between OH and NO is too slow for this mechanism to explain the magnitude of the observed OH^-.[31]

Figure 1(b) shows similar trends at 500 K, with the exception that the OH^- channel has a clear flat portion at $[e^-]_0$ below 10^{10} cm^{-3}, suggesting OH^- as a direct minor product of attachment to HNO_3. While the values are small resulting in significant scatter, the trend appears real, indicating that attachment to HNO_3 produces OH^- in 0.13% of reactions at 500 K, approximately the maximum that can be expected based on the endothermicity. We note that a single point at low $[e^-]_0$, as would be obtained in measuring product branching fractions in the traditional FALP technique, would not be enough to confirm this observation. The distinctive shape of the OH^- curve as a function of $[e^-]_0$ (Figure 1) is far stronger evidence, showing another utility of the VENDAMS method. At 500 K, it was not possible to derive a rate constant for attachment to OH due to the interplay between reactions (2) and (3) along with the unknown ion-ion mutual neutralization rate constant of OH^- with Ar^+.

Data from a "two-gas" VENDAMS experiment at 300 K appears in Figure 2. Here, a relatively large concentration of CCl_4 is added along with HNO_3 in order to yield a monatomic anion (Cl^-, via dissociative attachment to both CCl_4 and to the CCl_3 co-product) and to quickly deplete electron density such that the anion abundances evolve in time only through diffusion and mutual neutralization. The flat portions of the curves at low $[e]_0$ reflect the relative attachment rates to CCl_4 and HNO_3; because the concentrations of both species are known along with the attachment rate constant to CCl_4,[26,32] the attachment rate constant for reaction (1) is easily derived (Table I). The decrease in the abundance of NO_2^- and NO_3^- relative to Cl^- at higher $[e]_0$ is due to mutual neutralization, reaction (4). Derived rate constants (Table I) are similar

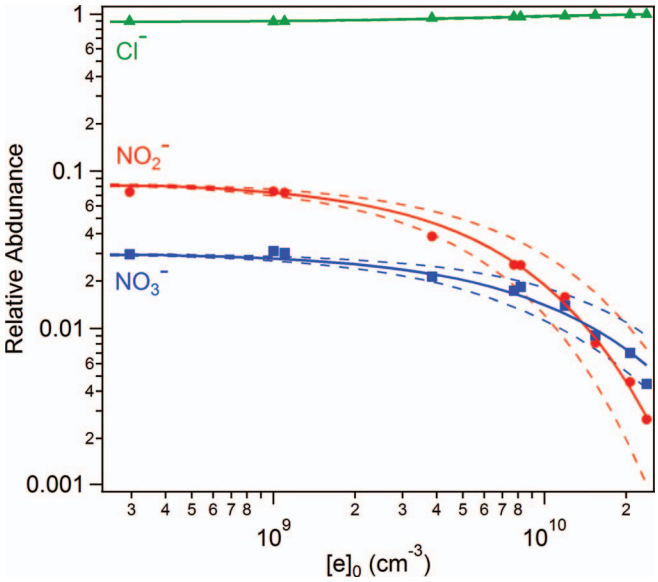

FIG. 2. "Two-gas" VENDAMS data (relative anion abundances after 4.6 ms reaction time vs. initial electron density) from addition of 3.8×10^9 cm^{-3} HNO_3 and 1.8×10^{10} cm^{-3} CCl_4 at 300 K. Experimental (points: NO_2^-, red circles; NO_3^-, blue squares; Cl^-, green triangles) and calculated (best-fit, solid lines; at uncertainty limits for $k_{NO_2^-} + Ar+$ and $k_{NO_3^-} + Ar+$, dashed lines; see Table I).

in magnitude to those measured for other mutual neutralization reactions.[28] The temperature dependence of the NO_2^- + Ar^+ reaction is $T^{-0.6}$, equal within uncertainty to the expected value of $T^{-0.5}$.[33] While in some instances VENDAMS data may yield information on products of neutralization, that is not possible here because none of the potential products (O, NO, or NO_2) attach thermal electrons rapidly. For NO_3^- neutralizing with Ar^+, the rate constants are not as well defined, particularly at 500 K. As a result, the measured temperature dependence is larger than expected ($T^{-1.4}$) but with large uncertainty.

TABLE I. Rate Constants derived in this study at 300 and 500 K.

	k (cm^3 s^{-1})	
	300 (K)	500 (K)
$e^- + HNO_3 \rightarrow$ products (weighted average)	$1.4 \pm 0.3 \times 10^{-7}$	$1.7 \pm 0.4 \times 10^{-7}$
$e^- + HNO_3 \rightarrow$ products (traditional method)	$1.3 \pm 0.4 \times 10^{-7}$	$1.8 \pm 0.7 \times 10^{-7}$
$e^- + HNO_3 \rightarrow$ products (VENDAMS, 2-gas)	$1.3 \pm 0.4 \times 10^{-7}$	$1.8 \pm 0.6 \times 10^{-7}$
$e^- + HNO_3 \rightarrow$ products (VENDAMS, 1 gas)	$1.8 \pm 0.8 \times 10^{-7}$	$1.4 \pm 0.8 \times 10^{-7}$
$\rightarrow NO_2 + OH^-$	$<5 \times 10^{-12}$	$1.9 \pm^{2.5}_{1.0} \times 10^{-10}$
$e^- + OH \rightarrow OH^-$	$1.2 \pm^{3}_{0.7} \times 10^{-11}$	$<4 \times 10^{-11}$
$NO_2^- + Ar^+ \rightarrow$ products	$5.2 \pm^{1.5}_{2.5} \times 10^{-8}$	$3.7 \pm 1.2 \times 10^{-8}$
$NO_3^- + Ar^+ \rightarrow$ products	$4.5 \pm 2.5 \times 10^{-8}$	$2.2 \pm 2 \times 10^{-8}$
$NO_2^- + Ar^+ + e \rightarrow$ products[a]	Best-fit $= 4 \times 10^{-19}$	$<1 \times 10^{-18}$

[a]cm^6 s^{-1}; no upper or lower limit at 300 K, only a most likely value; no lower limit at 500 K.

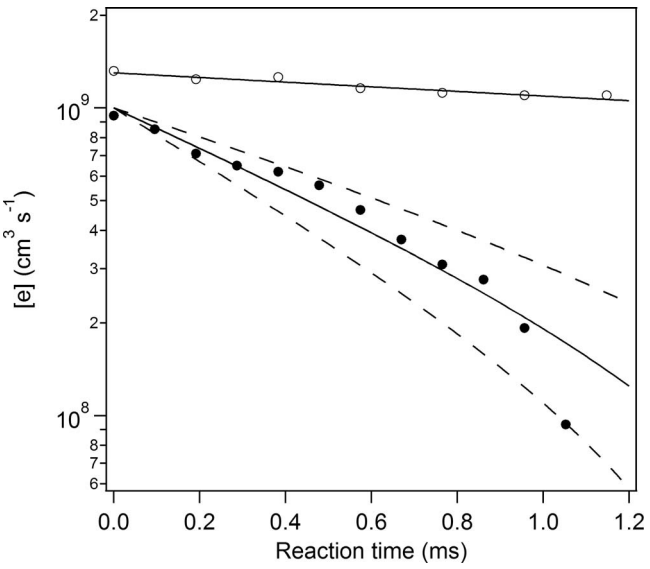

FIG. 3. Electron density as a function of reaction time with (solid circles) and without (open circles) 1×10^{10} cm^{-3} HNO_3 added to the afterglow. Solid lines are calculated electron densities assuming a diffusion rate of 175 s^{-1} and an electron attachment rate constant to HNO_3 of 1.3×10^{-7} cm^3 s^{-1}. Dashed lines are at the uncertainty limits for HNO_3 attachment reported in Table I.

The VENDAMS experiments are carried out on an unmodified FALP apparatus, allowing for measurements using the traditional FALP technique as well. Example data are shown in Figure 3 for the measurement of electron attachment to HNO_3, and derived attachment rate constants appear in Table I. The uncertainties of the measurement (∼25%) are typical for FALP electron attachment measurements.

Table I lists values of the rate constants derived from each experimental method employed in this study along with uncertainties. The overall rate constants for electron attachment to HNO_3 were measured by three independent methods. Both the traditional and two gas VENDAMS study yielded similar rate constants with similar errors, 1.3 and 1.8 $\times 10^{-7}$ cm^3 s^{-1} at 300 and 500 K, respectively. While those methods are the most straightforward and accurate, the one-gas VENDAMS also yields a value because the shapes of the anion abundances depend weakly on HNO_3 attachment rate constant; results from the "one-gas" method are consistent with the other values although with a larger uncertainty and a temperature dependence that is slightly negative instead of slightly positive. Table I lists an average of the three determinations weighted by the uncertainties. A small, positive temperature dependence is observed, although it is at our error limit. The collisional rate constants as calculated using extended Vogt-Wannier theory[26] are 4.3×10^{-7} and 3.4×10^{-7} cm^3 s^{-1} at 300 and 500 K, respectively, meaning that attachment occurs in roughly of 33% and 50% of collisions at these two temperatures. This increase in efficiency lies outside our error estimates.

Reaction (1) has been measured three times previously, with each study determining a lower rate constant of between 1.4–5 $\times 10^{-8}$ cm^3 s^{-1} at 300 K although with large uncertainty.[13,14,34] Two prior experiments using FALP apparatuses, one at Birmingham, the other at the National Oceanic and Atmospheric Administration (NOAA), both reported rate constants of 5×10^{-8} cm^3 s^{-1}. The Birmingham value was measured without any *in situ* monitor of the HNO_3 concentration.[13] As discussed in the Instrumental section, knowing the HNO_3 concentration accurately is difficult and it is likely that the amount of HNO_3 in the flow tube was lower than that determined exclusively by flow rate. At 500 K, the Birmingham experiments do not see attachment, which they interpreted as HNO_3 decomposition; however, the bond dissociation energy of HNO_3 is a considerable 2.1 eV,[13] well above the thermal energy distribution at 500 K. An alternative explanation for both the lower rate constant at 300 K and the lack of attachment at 500 K is reactivity on the inlet lines reducing the concentration of HNO_3 reaching the afterglow. In the NOAA study,[14] performed by following the increase in NO_2^- relative abundance, large corrections due to differences in diffusion rates between positive ion - electron plasmas and ion-ion plasmas had to be made leading to large error bars (60%). That measurement used reaction (6) to monitor the HNO_3 concentration and therefore we speculate that most of the difference between the NOAA result and the present measurements is due the diffusional corrections being even larger than estimated (in the present experiments, the plasma diffusion is directly measured). In any case, considering the difficulty of these experiments the factor of 2.5 agreement with the current result is satisfactory.

The experimental electron attachment results are limited to thermal conditions between 300–500 K and pressures around 1 Torr. Ongoing work to develop a "kinetic modeling" approach to electron attachment processes appears sufficiently vetted to be used to extrapolate from the experimental data to other conditions with some degree of confidence.[35–38] Kinetic modeling treats the attachment by separating it as fully as possible into discrete steps and then treating each of those steps using statistical theory. First, the attaching neutral and incident electron form a "contact pair," which may decay either through elastic or inelastic scattering or through capture to form a vibrationally excited anion, HNO_3^{-*}, with internal energy equal to the sum of the thermal energy of the HNO_3 and the kinetic energy of the incident electron. The probability of capture is calculated through analytical approximations of extended Vogt-Wannier[26,30,39] theory adjusted by empirically fit factors to account for the finite time scale required to incorporate the incident electron into the electron cloud of the molecule, the existence of any energetic barrier between the neutral and anionic potential surfaces, and any increase in the scattering cross section due to vibrational excitation of the neutral. Subsequently, the vibrationally excited anion may be stabilized either through electron autodetachment, inelastic collisions yielding the parent anion, or dissociation yielding a fragment anion, all of which may be modeled using statistical theory. In the case of HNO_3^{-*}, the significant exothermicity of dissociation to $OH + NO_2^-$ results in a branching fraction of essentially one, greatly simplifying the analysis in that the calculation of the rate constant of the formation of HNO_3^{-*} is equivalent to the experimentally observed attachment rate constant to HNO_3.

Fitting the experimental HNO_3 attachment rate constants at 300 and 500 K requires essentially no reduction of the

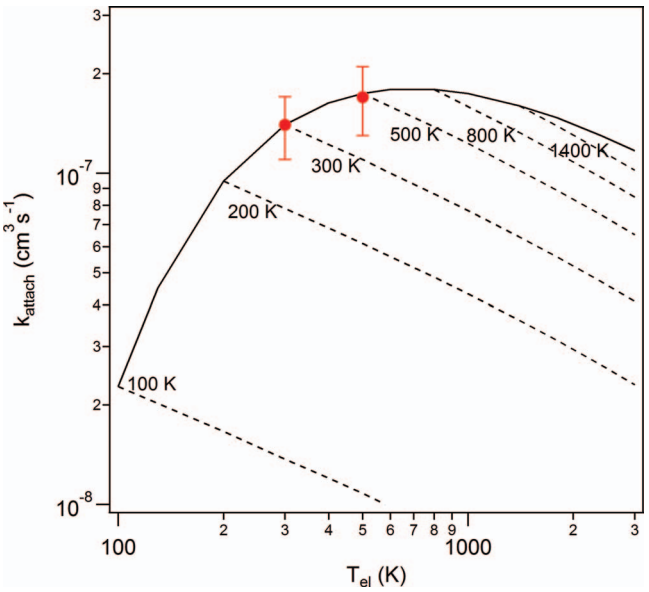

FIG. 4. Experimental (points) and extrapolated (see text and Refs. 35, 36, and 38 for details of kinetic modeling; $c_1 = 0.25$, $c_2 = 0$, $E_{n,0} = 0.03$ eV, isotropic polarizability = 3.5 Å^3, dipole moment = 2.17 D) dissociative electron attachment rate constants to HNO_3 as a function of electron temperature, T_{el}. Modeled rate constants are for non-thermal conditions (dashed lines) at the indicated gas temperatures, or thermal conditions (solid line).

Vogt-Wannier capture probabilities due to either inefficiency of electron-phonon coupling or increased likelihood of vibrational excitation for energetic electrons (in the language of Ref. 35 both c_1 and c_2 are approximately 0). Inclusion in the model of a modest barrier of 200–400 cm^{-1} between the neutral and anion surfaces results in the observed rate constants being moderately lower than calculated collision rate constants and having a small, positive temperature dependence. The existence of an energetic barrier is consistent with the observed increase in attachment efficiency at 500 K; the higher temperature behavior of a system lacking a barrier would be dominated by the decreased cross section for capture of energetic electrons and would show a decreased efficiency. Extrapolations to conditions inaccessible with the experiment using kinetic modeling with the parameters best-fit to the experimental points are shown in Fig. 4.

The data give little information on the absolute rate of the dissociation of HNO_3^-; however, assuming statistical behavior, the observed branching ratio between reaction (1) (NO_2^- + OH) and reaction 2 (OH^- + NO_2) at 500 K does reasonably constrain the branching ratio at other temperatures. Employing the simplified statistical adiabatic channel model,[40–42] a series of specific dissociation rate curves can be calculated for reaction (1), ranging between the orbiting transition state-phase space limit[43] at the high end, and a curve that rises more slowly at low internal energies and approaches rigid-activated complex Rice-Ramsperger-Kassel-Marcus behavior at higher internal energies.[44] For each of these curves, or any at rates in between, the single 500 K data point defines a specific rate curve for reaction (2); the ratio of these two curves integrated across the internal energy distribution of HNO_3^{-*} at a given temperature gives the branching ratio for electron attachment to HNO_3 at that temperature. Although the absolute rate of the dissociations varies between these limits, the derived branching ratios vary little, only by about a factor of two, with results given in Table II. The calculations support the observation of reaction (2) at 500 K, but not at 300 K; the calculated fraction of HNO_3^{-*} with internal energy above the threshold to reaction (2) is negligible at 300 K, but over ten percent at 500 K.

TABLE II. Calculated kinetics of $HNO_3 + e^- \rightarrow OH^- + NO_2$.

Temperature (K)	Fraction of HNO_3^{-*} above energetic threshold[a]	Branching fraction[b]
300	0.003	6×10^{-5}
500	0.13	1.3×10^{-3}
700	0.41	5×10^{-3}
1000	0.77	0.03

[a]Calculated using the kinetic modeling approach (see text) assuming a nuclear barrier $E_{n,0} = 0.03$ eV. HNO_3^{-*} is the excited anionic state formed upon electron capture.
[b]Calculated using the statistical adiabatic channel model (see text). Uncertainties are a factor of two, except at 500 K, see Table I.

The electron attachment rate constant to OH, reaction (3), is also measured. The effective two body rate at 300 K is $1.2\pm^{3}_{0.7} \times 10^{-11}$ cm^3 s^{-1} and at 500 K, only an upper limit can be derived. Assuming third order kinetics, the three-body rate constant is 3.7×10^{-28} cm^6 s^{-1}. While VENDAMS has been used to measure a pressure dependence of a radical produced in a primary attachment,[36] a similar attempt for OH failed due to the large uncertainties associated with the small rate. The three-body rate constant is considerably faster than associative attachment to other diatomics, O_2 and NO, which have values between 10 to 10^4 times smaller depending on the nature of the buffer gas.[45,46] Assuming OH^{-*} is formed with similar efficiency to O_2^{-*} or NO^{-*}, the observed attachment rate, would be significantly faster than for O_2 or NO as the considerably greater electron affinity of OH would result in a slower autodetachment. However, it has been speculated that electron capture to form OH^{-*} should be slow due to the lack of a low-lying crossing between the neutral and anionic potential surfaces.[46]

Finally, a small amount of information on electron catalyzed mutual neutralization of NO_2^- with Ar^+ (process (5)) is obtained. The best-fit value is about 4×10^{-19} cm^6 s^{-1}. However, the error analysis indicates that all values allowed led to acceptable fits. Thus, there is a most probable value but a wide range of values are satisfactory.

SUMMARY

The present study uses three different data acquisition methods in a flowing afterglow to measure a variety of plasma kinetics initiated by electron attachment to HNO_3. All three methods, the traditional FALP technique and both one- and two-gas VENDAMS experiments, were used to measure the primary electron attachment rate constant. The values agreed well with each other and indicate previous results for this reaction were too small by a factor of 2 to 10. In addition, the VENDAMS study showed that there is a small endothermic channel producing OH^-, previously unobserved using traditional methods. VENDAMS also allows studies of attachment

to the radical neutrals formed in the initial attachment. Here we have been able to determine the rate constant for attachment to the OH formed in attachment to HNO_3. Finally, we have added to our database of ion-ion mutual neutralization kinetics, with rate constants for both NO_2^- and NO_3^- neutralizing with Ar^+.

ACKNOWLEDGMENTS

This project was supported by the Air Force Office of Scientific Research through AFOSR (Contract No. 2303EP). T.M.M. is under contract (FA8718-10-C-0002) from the Institute for Scientific Research of Boston College.

[1]E. E. Ferguson, F. C. Fehsenfeld, and A. L. Schmeltekopf, in *Advances in Atomic and Molecular Physics*, edited by D. R. Bates (Academic, New York, 1969), Vol. 5, pp. 1–56.
[2]E. E. Ferguson, J. Am. Soc. Mass Spectrom. **3**, 479–486 (1992).
[3]S. T. Graul and R. R. Squires, Mass Spectrom. Rev. **7**, 263 (1988).
[4]T. M. Miller, J. F. Friedman, J. S. Williamson, L. C. Schaffer, and A. A. Viggiano, Rev. Sci. Inst. **80**, 034104 (2009).
[5]T. M. Miller, Adv. At., Mol., Opt. Phys. **51**, 299–342 (2005).
[6]M. Larsson and A. E. Orel, *Dissociative Recombination of Molecular Ions* (Cambridge University Press, Cambridge, 2008).
[7]D. Smith and N. G. Adams, in *Physics of Ion-Ion and Electron-ion Collisions*, edited by F. Brouillard and J. W. McGowan (Plenum, New York, 1983), p. 501.
[8]R. Johnsen, E. V. Shun'ko, T. Gougosi and M. F. Golde, Phys. Rev. E **50**(5), 3994–4004 (1994).
[9]J. C. Bopp, T. M. Miller, A. A. Viggiano, and J. Troe, J. Chem. Phys. **129**, 074308 (2008).
[10]N. S. Shuman, T. M. Miller, C. M. Caples, and A. A. Viggiano, J. Phys. Chem. A **114**, 11100 (2010).
[11]N. S. Shuman, T. M. Miller, N. Hizari, E. D. Luzik, and A. A. Viggiano, J. Chem. Phys. **133**, 234304 (2010).
[12]N. S. Shuman, T. M. Miller, R. J. Bemish, and A. A. Viggiano, Phys. Rev. Lett. **106**, 018302 (2011).
[13]N. G. Adams, D. Smith, A. A. Viggiano, J. F. Paulson, and M. J. Henchman, J. Chem. Phys. **84**, 6728 (1986).
[14]F. C. Fehsenfeld, C. J. Howard, and A. L. Schmeltekopf, J. Chem. Phys. **63**(7), 2835 (1975).
[15]M. W. Chase, Jr., J. Phys. Chem. Ref. Data **9**, 1344 (1998).
[16]K. M. Ervin, J. Ho and W. C. Lineberger, J. Phys. Chem. **92**, 5405 (1988).
[17]J. R. Smith, J. B. Kim, and W. C. Lineberger, Phys. Rev. A **55**, 2036 (1997).
[18]T. M. Miller, A. E. S. Miller, J. F. Paulson, and X. Liu, J. Chem. Phys. **100**, 8841 (1994).
[19]D. Smith and P. Spanel, Adv. At., Mol. Opt. Phys. **32**, 307–343 (1994).
[20]N. S. Shuman, T. M. Miller, A. A. Viggiano, and J. Troe, "Teaching an old dog new tricks: Using the flowing afterglow to measure kinetics of electron attachment to radicals, ion-ion mutual neutralization, and electron catalyzed mutual neutralization," Adv. At., Mol., Opt. Phys. (in press).
[21]J. O. Ballenthin, W. F. Thorn, T. M. Miller, A. A. Viggiano, D. E. Hunton, M. Koike, Y. Kondo, N. Takegawa, H. Irie, and H. Ikeda, J. Geophys. Res. **108**, ACH7-1-7-1, doi:10.1029/2002JD002136 (2003).
[22]L. G. Huey, E. J. Dunlea, E. R. Lovejoy, D. R. Hanson, R. B. Norton, F. C. Fehsenfeld, and C. J. Howard, J. Geophys. Res. **103**, 3355–3360, doi:10.1029/97JD02214 (1998).
[23]T. Su and W. J. Chesnavich, J. Chem. Phys. **76**, 5183–5185 (1982).
[24]D. K. Bohme, in *Interactions Between Ions and Molecules*, edited by P. Ausloos (Plenum, New York, 1975), pp. 489–504.
[25]S. J. Burns, J. M. Matthews, and D. L. McFadden, J. Phys. Chem. **100**, 19436 (1996).
[26]E. I. Dashevskaya, I. Litvin, E. E. Nikitin, and J. Troe, Phys. Chem. Chem. Phys. **10**, 1270 (2008).
[27]M. J. Church and D. Smith, J. Phys. D **11**, 2199 (1978).
[28]T. M. Miller, N. S. Shuman, and A. A. Viggiano, "Behavior of rate coefficients for ion-ion mutual neutralization, 300–550 K," J. Chem. Phys. (submitted).
[29]N. S. Shuman, T. M. Miller, J. F. Friedman, A. A. Viggiano, S. Maeda, and K. Morokuma, J. Chem. Phys. **134**, 094310 (2011).
[30]E. I. Dashevskaya, I. Litvin, E. E. Nikitin, and J. Troe, J. Phys. Chem. A **115**, 6825–6830 (2011).
[31]R. Atkinson, D. L. Baulch, R. A. Cox, R. F. Hampson, J. A. Kerr, M. J. Rossi, and J. Troe, J. Phys. Chem. Ref. Data **26**, 1329–1499 (1997).
[32]R. G. Levy, S. J. Burns, and D. L. McFadden, Chem. Phys. Lett. **231**, 132 (1994).
[33]A. P. Hickman, J. Chem. Phys. **70**, 4872 (1979).
[34]D. Wecker and R. N. Schindler, Z. Naturforsch. **39A**, 542 (1984).
[35]J. Troe, T. M. Miller and A. A. Viggiano, J. Chem. Phys. **127**, 244303 (2007).
[36]N. S. Shuman, T. M. Miller, J. F. Friedman, A. A. Viggiano, A. I. Maergoiz, and J. Troe, J. Chem. Phys. **135**, 054306 (2011).
[37]J. Troe, G. Marowsky, N. S. Shuman, T. M. Miller, and A. A. Viggiano, Z. Phys. Chem. **225**, 1405–1416 (2011).
[38]J. Troe and E. E. Nikitin, "On the kinetic modeling of electron attachment to polyatomic molecules," Mol. Phys. (in press).
[39]I. I. Fabrikant and H. Hotop, Phys. Rev. A **63**, 022706 (2001).
[40]J. Troe and V. G. Ushakov, J. Phys. Chem. A **110**(21), 6732–6741 (2006).
[41]W. R. Stevens, B. Sztaray, N. S. Shuman, T. Baer, and J. Troe, J. Phys. Chem. A **113**(3), 573–582 (2008).
[42]J. Troe, Z. Phys. Chem. **223**(4-5), 347–357 (2009).
[43]W. J. Chesnavich and M. T. Bowers, J. Chem. Phys. **66**, 2306–2315 (1977).
[44]A. Bodi, A. Kvaran, and B. Sztaray, J. Phys. Chem. A **115**, 13443–13451 (2011).
[45]L. G. Christophorou, (Academic, New York, 1984).
[46]G. E. Caledonia, Chem. Rev. **75**, 333–351 (1975).